Simultaneous observations of a polar cap sporadic-e layer by twin incoherent scatter radars at resolute

Wang, Yong; Themens, David R.; Wang, Cheng; Ma, Yu Zhang; Reimer, Ashton; Varney, Roger; Xing, Zan Yang; Zhang, Qing He; Jayachandran, P. T.

DOI:
10.1029/2022JA030366

JGR Space Physics

RESEARCH ARTICLE
10.1029/2022JA030366

Special Section:
The Arctic: An AGU Joint Special Collection

Simultaneous Observations of a Polar Cap Sporadic-E Layer by Twin Incoherent Scatter Radars at Resolute

Yong Wang[1], David R. Themens[2,3], Cheng Wang[4], Yu-Zhang Ma[1], Ashton Reimer[5], Roger Varney[5], Robert Gilies[6], Zan-Yang Xing[1], Qing-He Zhang[1], and P. T. Jayachandran[2]

[1]Shandong Provincial Key Laboratory of Optical Astronomy and Solar-Terrestrial Environment, School of Space Science and Physics, Institute of Space Sciences, Shandong University, Weihai, China, [2]Physics Department, University of New Brunswick, Fredericton, NB, Canada, [3]School of Engineering, Space Environment and Radio Engineering Group (SERENE), University of Birmingham, Birmingham, UK, [4]Qian Xuesen Laboratory of Space Technology, Chinese Academy of Space Technology, Beijing, China, [5]Center for Geospace Studies, SRI International, Menlo Park, CA, USA, [6]Department of Physics and Astronomy, University of Calgary, Calgary, AB, Canada

Key Points:

- An amazing example of polar cap Es layer is first presented by the twin radars of northward-looking face of Resolute Incoherent-Scatter Radar and Resolute Incoherent-Scatter Radar-Canada at Resolute, Canada simultaneously
- The morphology of the polar cap Es layer is comprehensively furthered, interpreting the horizontal scale size (>350 km) and double layers
- To reasonably explain this phenomenon, a new process is hypothesized, consisting of localized electric field and gravity wave

Correspondence to:
Q.-H. Zhang,
zhangqinghe@sdu.edu.cn

Citation:
Wang, Y., Themens, D. R., Wang, C., Ma, Y.-Z., Reimer, A., Varney, R., et al. (2022). Simultaneous observations of a polar cap Sporadic-E layer by twin incoherent scatter radars at resolute. *Journal of Geophysical Research: Space Physics*, *127*, e2022JA030366. https://doi.org/10.1029/2022JA030366

Received 7 FEB 2022
Accepted 17 MAY 2022

Abstract At high latitudes, the Sporadic-E layer (Es layer) is a common phenomenon but is still poorly understood due to sparse measurements and the difficulty of conventional mechanisms to operate. In this study, an interesting case of polar cap Es layer is first studied by using the twin incoherent scatter radars (northward-looking face of Resolute Incoherent-Scatter Radar and Resolute Incoherent-Scatter Radar-Canada), a Canadian Advanced Digital Ionosonde, and a Magnetometer, all at Resolute, Canada. From several electron density profiles of the twin radars, the horizontal scale of the polar cap Es layer is found to be greater than 350 km. Moreover, the polar cap Es layer is determined to be drifting from the bottom F region (>150 km) to the lower E region. Furthermore, a unique appearance of double polar cap Es layers is observed. As a result, these peculiar signatures inspire a newly proposed process that involves the combination of localized electric fields and gravity waves.

Plain Language Summary The Sporadic-E layer (Es layer) is a globally common phenomenon, which is comprehensively and unceasingly studied in decades by using the observation measurements and numerical simulations. The remarkable agreements on the characteristics and generation mechanisms of Es layer at middle latitudes have then been almost achieved. However, over the polar region, it is still poorly understood due to sparse measurements and the difficulty of conventional mechanisms to operate. In this study, an interesting case of polar cap Es layer are first reported by using the twin radars of northward-looking face of Resolute Incoherent-Scatter Radar and Resolute Incoherent-Scatter Radar-Canada, Canadian Advanced Digital Ionosonde, and Magnetometer simultaneously. Through comprehensively studies, the understanding of polar cap Es layer is clearly extended, not only on the characteristics but also on the mechanism processes. The polar cap Es layer is horizontally greater than 350 km; a new process on the generation mechanism is provoked including the functions of particle precipitation and gravity wave. As a consequence, we present a peculiar evidence for the first time to greatly enrich our knowledge on the polar cap Es layer, showing us a new insight on it.

1. Introduction

The Sporadic-E (Es) layer is a common thin layer of plasma that occurs at the heights of 90–140 km, usually with peak density generally constituted by metallic ions of Fe^+, Mg^+, and Na^+ et al. (e.g., Behnke & Vickery, 1975; Bedey & Watkins, 1996, 1998; Narcisi, 1971; Turunen et al., 1988). These ions are theorized to be produced by the meteor ablation into the ionosphere, possessing a much longer lifetime due to their much lower recombination rate (e.g., Shinagawa et al., 2017; and references in) than the main ion species (e.g., NO^+ and O_2^+) in the E region. As a result, they can be massed into a thin layer that can last a couple of hours. Regarding the tricky process to compress the Es layer, several generation mechanisms have been proposed, fundamentally containing the neutral wind and/or electric field and/or gravity wave (e.g., Behnke & Vickery, 1975; Bristow & Watkins, 1993; Kumar & Hanson, 1980; MacDougall & Jayachandran, 2005; MacDougall et al., 2000b).

In decades, the studies dealing with the characteristics of thin Es layers have been continued, which were carried out by using a large number of instruments, such as ionosondes, incoherent scatter radars, high-frequency radars,

radio-occultation techniques, as well as GPS receivers (e.g., Bristow & Watkins, 1993; Chen et al., 2021; Fukao et al., 1998; Larsen et al., 2007; MacDougall et al., 2000a; Maeda & Heki, 2014; 2015; Maeda et al., 2016; Sun et al., 2018, 2020, 2021; Wang, Jayachandran, et al., 2021; Wu et al., 2005; Yeh et al., 2014). Recently, at middle latitudes, Maeda and Heki (2014); Maeda et al. (2016) and Maeda and Heki (2015) attempted to fundamentally illustrate the horizontal structure of the Es layer by 2-dimensional Total Electron Content maps drawn from the dense GPS receivers over Japan, generally concluding that the Es layer was spanning over ∼150 km in length and ∼30 km in width and was propagating in different directions. Moreover, benefiting from a broader region over China, Sun et al. (2018, 2020, 2021) carried out several tests to further understand the morphological characteristics of the Es layer by using the combined instruments of dense GPS receivers and radars. They reported that the Es layer was generally shown as a band-like structure along with different directions with a much greater scale of 1,000–3,000 km and likely drifted southwestward at speed of 30–210 m/s.

At high latitudes, only a few studies up to now focused on the morphological structures of the Es layer due to limited measurements. Bristow and Watkins (1993) studied the densities and temperatures of E-region thin metallic ion layers by incoherent scatter radar observations with a height resolution of 300 m. Hysell et al. (2014) reported the ionospheric Es layer in the daytime by a 30 MHz radar in Alaska, detecting the patchy structure of ∼10 km sale size with a slow ropagation. Recently, Wang, Jayachandran, et al. (2021) simply mentioned the horizontal structure of the polar cap Es layer by using the multi-beams of northward-looking face of Resolute Incoherent-Scatter Radar (RISR-N) at Resolute Bay station, Canada. Chen et al. (2021) inferred that the Es layer over Antarctica was in the form of bands along a specific direction but without directly observation evidence. As a consequence, it is still a long way to study the polar cap Es layer in detail, compared with the abundant investigations at middle latitudes.

Fortunately, Resolute provides a rare opportunity to determine the morphological characteristics of the polar cap Es layer through combined measurements of various instruments to probing the ionosphere. This includes the RISR-N, Resolute Incoherent-Scatter Radar-Canada (RISR-C), Canadian Advanced Digital Ionosonde (CADI), and Magnetometer. In this study, we will first introduce the instruments involved in our examination. Then, an interesting example of the polar cap Es layer is presented using the measurements from instruments (RISR-N, RISR-C, CADI, and Magnetometer) followed by discussions and conclusions.

2. Instruments

The Resolute Bay (74.75°N, 265.0°E in geographic coordinate; 82.9°N magnetic latitude [MLat]), which is in the middle of the polar cap, hosting various instruments for ionospheric monitoring. We use the two incoherent scatter radars (RISR-N and RISR-C), CADI and the magnetometer measurements for this study.

The twin incoherent-scatter radars of RISR-N and RISR-C are the cornerstones of imaging facilities that provide key information about Earth's space environment and their effects on the upper atmosphere and technology. They point in opposite directions, RISR-N to the north and RISR-C to the south, providing ionospheric parameters across a vast swath of sky. These two radars are possessing multiple electronically steerable beams under a set of working modes, almost simultaneously offering multiple profiles of electron density (Ne) and electron temperature (Te) and ion temperature (Ti), and ion velocity (Vi) along the line-of-sight direction. Note that the beam width of the twin radars is ∼1.1°. If both adopt the Alternating Code (AC 16–30) mode, the twin radars can provide the observation measurements in the lower E region with an altitude resolution of ∼4 km and a cadence of 1 or 3 min in more than 20 beams, definitely covering a vast region. The region of the ionosphere covered by the radars is shown in Figure 1. The Resolute CADI is run by the Canadian High Arctic Ionospheric Network (Jayachandran, Langley, et al., 2009), providing both ionograms in a cadence of 1 min and fixed frequency drift measurements at a resolution of 30 s. In this paper, the 4.0 MHz echoes will be used in Section 3.

Underlying solar wind and Interplanetary Magnetic Field (IMF) conditions were extracted from the OMNI-2 website, which all had already been time-shifted to the nose of bow shock. To account for the propagation delay of solar wind and IMF changes from the nose of bow shock to the polar ionosphere, an additional 7 min was added, which is consistent with the previous results (e.g., Liou et al., 1998; Wang, Cao, et al., 2021). The variation of magnetic field at Resolute Bay is provided by the Resolute magnetometer, which was obtained from the SuperMAG, as well as the auroral electrojet indices of SME/SMU/SML (Newell & Gjerloev, 2011a). SuperMAG is a worldwide collaboration of organizations and national agencies that currently operate more than 300

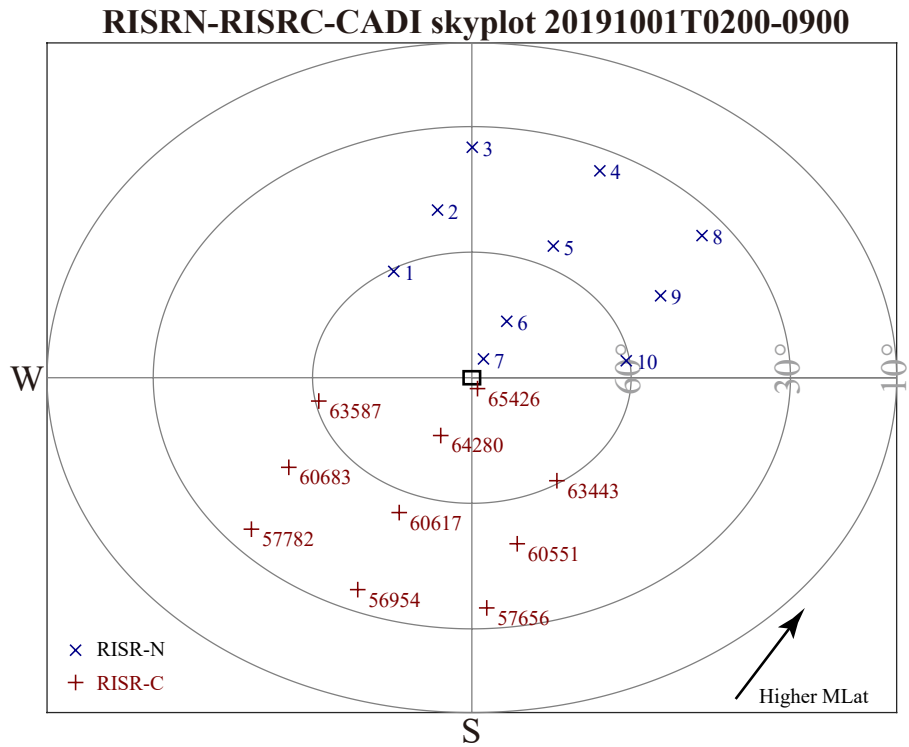

Figure 1. The distributed manner of involved instruments at Resolute Bay station as a function of elevation and azimuth angles, including the phased-array beams of northward-looking incoherent scatter radar (northward-looking face of Resolute Incoherent-Scatter Radar [RISR-N], the blue crosses with each number), Resolute Incoherent-Scatter Radar-Canada (RISR-C, the red pluses with a number), CADI (the black square in the center), and the magnetometer (shared the same location of CADI). The black concentric circles represent the elevation angles of 10°, 30°, and 60°, respectively. During the conducted period, the black arrow at the right-bottom corner directs the higher magnetic latitude (MLat).

ground-based magnetometers, providing easy access to validated ground magnetic field perturbations in the same coordinate system with a common baseline removal approach (Newell & Gjerloev, 2011a, 2011b).

3. Observations and Results

3.1. The Configurations of Radar Beams in the Experiment

Figure 1 shows the pattern of multiple beams of these two incoherent radars and CADI and magnetometer as a function of elevation and azimuth angles. The north is on up, west is at left. The black circles represent elevations of 10°, 30°, and 60°, respectively. The blue crosses with a number (on top) orderly mark Beams 1–10 from RISR-N. Similarly, the red pluses along with code (at the bottom) respectively represent Beams 56954/57656/57782/60617/60551/60683/63443/63587/64280/65426 of RISR-C. In the center of Figure 1, the bold black square indicates the location of CADI and magnetometer, which is close to Beam 7 of RISR-N and Beam 65426 of RISR-C. The black arrow in the right bottom corner is pointing from low MLat to high MLat during the conducted experiment period.

3.2. IMF Conditions and Solar Wind and Geomagnetic Indices

Figure 2 overviews the IMF conditions and solar wind and geomagnetic data during the period 02:00–09:00 UT on 1 October 2019, during which an interesting phenomenon of polar cap Es layer occurred. Figures 2a and 2b show the IMF components and solar wind dynamic pressure, including the IMF Bx (blue), By (black), and Bz (red) components under Geocentric Solar Magnetic coordinates (a); and dynamic pressure (P_{Dyn}; b). Figure 2c represents the SYM-H index collected from World Data Center at Kyoto. Figure 2d presents the Auroral Electrojet Indices obtained from SuperMAG, SME in red, SML in gray, and SMU in blue, respectively. Figure 2e shows

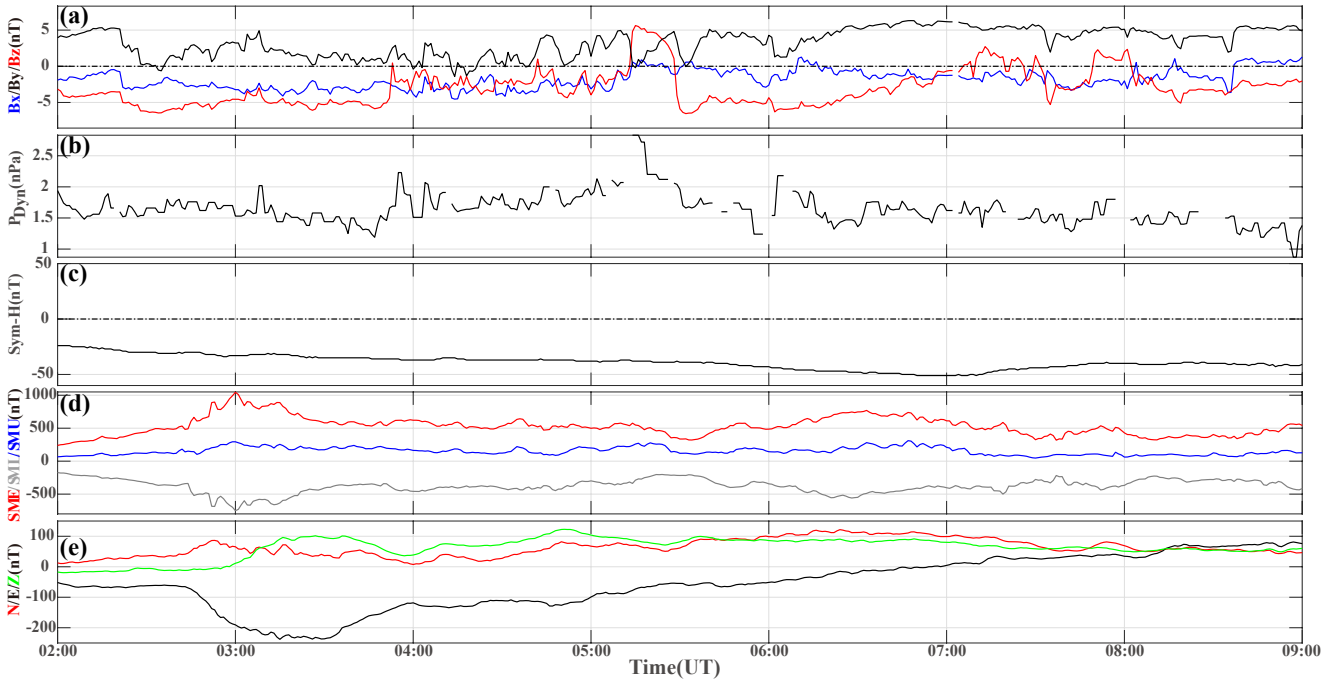

Figure 2. Overviews the solar wind and interplanetary magnetic field (IMF) conditions and geomagnetic indices. Panels (a and b) show the solar wind and IMF conditions, (a) IMF Bx (blue), By (black), and Bz (red) components, (b) the solar wind dynamic pressure. The data were obtained from OMNI website and have been delayed 7 min to approximately allow the spread from the nose of bow shock to the polar ionosphere. Panels (c) presents the SYM-H (Dst) index, which was required from the World Data Center. Panel (d) lists the auroral electrojet indices of SME (red), SMU (blue), and SML (gray). Panel (e) represents the variation of local magnetic field over Resolute in three directions of Northward (N, red), Eastward (E, black), and downward (Z, green). The data in Panels (d and e) was collected from the SuperMAG.

the perturbations of the local magnetic field along 3 directions observed by the magnetometer at Resolute, N for magnetic northward (red), E for the magnetic eastward (black), and Z for downward (green). Note that these variations of the magnetic field are the differences between the magnetic field values and the averaged baseline during 1 day.

The IMF Bz component (the red line in Figure 2a) is generally negative (southward) around −5 nT with several positive (northward) transitions at ∼05:15–05:30 UT and 07:10–07:30 UT and 07:50–08:00 UT. Similarly, the IMF Bx component (the blue line in Figure 2a) is almost weak negative, comprising a small number of positives within the second half period. While the IMF By component (the black line in Figure 2a) is always positive (∼4 nT) the whole time except for a few negative perturbations during the former period. The solar wind dynamic pressure (Figure 2b) is almost stable below 2.5 nPa during the period of interest. The SYM-H index in Figure 2c is gently decreasing from −22 to −50 nT and then is recovering to −40 nT, suggesting the faintly disturbing condition of geomagnetic activity. Meanwhile, the Auroral Electrojet Indices of SML in Figure 2d is quickly rushing to ∼−800 nT at 03:00 UT from a quiet condition (before 02:40 UT) and then is fluctuating around −500 nT, probably indicating the strong to moderate substorms that happened at the nightside.

Furthermore, the variations of the local magnetic field are worthy of attention. The components of *N*/Z (red/green lines in Figure 2e, respectively) are almost fluctuating between 0 and 100 nT, respectively going up to 100 nT and then slowly decreasing to 50 nT from ∼02:40 UT to 07:40 UT. On the contrary, the E component (black line in Figure 2e) sharply decreases initially at ∼02:40 UT from −60 to −240 nT at 03:30 UT and then recovers gradually, clearly representing the westward perturbation of the magnetic field. Considering the nightside distribution of this experiment, the disturbance is likely produced by a weak upward current during this interval (e.g., Wang et al., 2010). It is exciting to point out that the started time of disturbance coincides with the initial period of the polar cap Es layer closely.

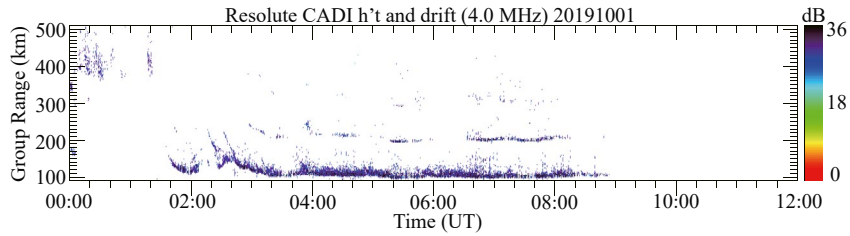

Figure 3. Sequence of group range at 4 MHz by Canadian Advanced Digital Ionosonde (CADI) at Resolute Bay station during the interval of interest of 00:00–12:00 UT on 1 October 2019 between the virtual height of 100–500 km.

3.3. The Characteristics of Polar Cap Es Layer

Figure 3 shows a group range of reflected echoes on a fixed frequency of 4.0 MHz from Resolute CADI during a period of 00:00–12:00 UT on 1 October 2019. The color bar on the right-hand side represents the power of received echoes. In Figure 3, below the virtual height of 200 km, a clear band of strong echoes (∼30 dB) shows up between 01:40 UT and 09:00 UT. Above this height, there are two more equally separated weak bands of echoes, which are the second and third hop reflections from the lowest layer. Note that the virtual height is slightly greater than their true height. In practice, the strong structure can be separated into two groups at around 02:40 UT according to their differentiated actions. In the former period of 01:40–02:40 UT, the echoes are initially descending and then rising again quickly, which is typically to layers associated with particle precipitation (e.g., Jayachandran, Hosokawa, et al., 2009, Jayachandran et al., 2017). This view is supported by the observations of incoherent-scatter radars (next paragraph). During the latter interval of 02:40–09:00 UT, the dynamics of thin layer are quietly different from that in the former period, the height of the layer decreased from ∼150 to 120 km at around 03:20 UT and then lasted a quite long time (>6 hr) around at 110 km. The latter layer is the polar cap Es layer (e.g., Wang, Jayachandran, et al., 2021). During the period (00:00–01:20 UT), a cloud of weak echoes occurs at almost above 350 km, representing the ionospheric information of F region (beyond the scope of this article). Furthermore, we have also checked the ionograms of Resolute CADI in a cadence of 1 min (not shown here), definitely demonstrating the polar cap Es layer.

The polar cap Es layer, observed by the CADI, is recorded by multi-beams of twin radars of RISR-N and RISR-C. Figure 4 shows 20 profiles of electron density from different radar beams during a period of 02:00–09:00 UT on 1 October 2019. The top panels show RISR-N and the bottom panels show RISR-C profiles. These are arranged by following the beam patterns depicted in Figure 1. The beam number is labeled in the top-right corner along with the corresponding azimuth and elevation angles. RISR-N panels in magenta and RISR-C panels are in red. The color bar on the right-hand side represents the electron density scale. Generally speaking, there is a clear high electron density structure between the altitude range of 120–95 km during a period of 02:40–09:00 UT from almost all panels of Figure 4 simultaneously, which is definitely supportive evidence on the polar cap Es layer. Initially, the polar cap Es layer is gently falling down from 120 to 105 km in altitude and then is sustaining a long time peacefully from 03:20 UT, which are identical to the behavior of the CADI data shown in Figure 3. Note that during the whole period the polar cap Es layer has been interrupted several times especially from RISR-N panels (i.e., Beam 1 within 05:00–06:00 UT). In Figure 4, the polar cap Es layer from RISR-C panels (bottom) is broadly stronger than the one by RISR-N panels. If we compare the intensity of the polar cap Es layer from bottom rows to top carefully, the polar cap Es layer is almost gradually weakening. During the period, the Resolute station is approximately at local midnight. The MLat from the bottom panels to the top of Figure 4 is increasing, as shown by the black arrow in the right-bottom corner of Figure 1. Thus, the density distribution of the polar cap Es layer depends on the MLat, stronger at the lower MLat, possibly implying the spread characteristics of metallic ions. Additionally, within the period of 02:00–03:00 UT, an enhanced electron density is directly penetrating from the altitude above 140–110 km by a large number of profiles in Figure 4 in particular from RISR-C panels (e.g., Beam 63587, 60683, 57782), clearly suggesting the particle precipitation, which is suitably consistent with the result of Figure 3.

Furthermore, the specific configuration of these beams from the twin radars as shown in Figures 1 and 4 provides a chance to discover the scale size of the polar cap Es layer in 2-dimension. In this experiment, 20 electron density profiles simultaneously record the polar cap Es layer. Then, the maximumly horizontal distance between these

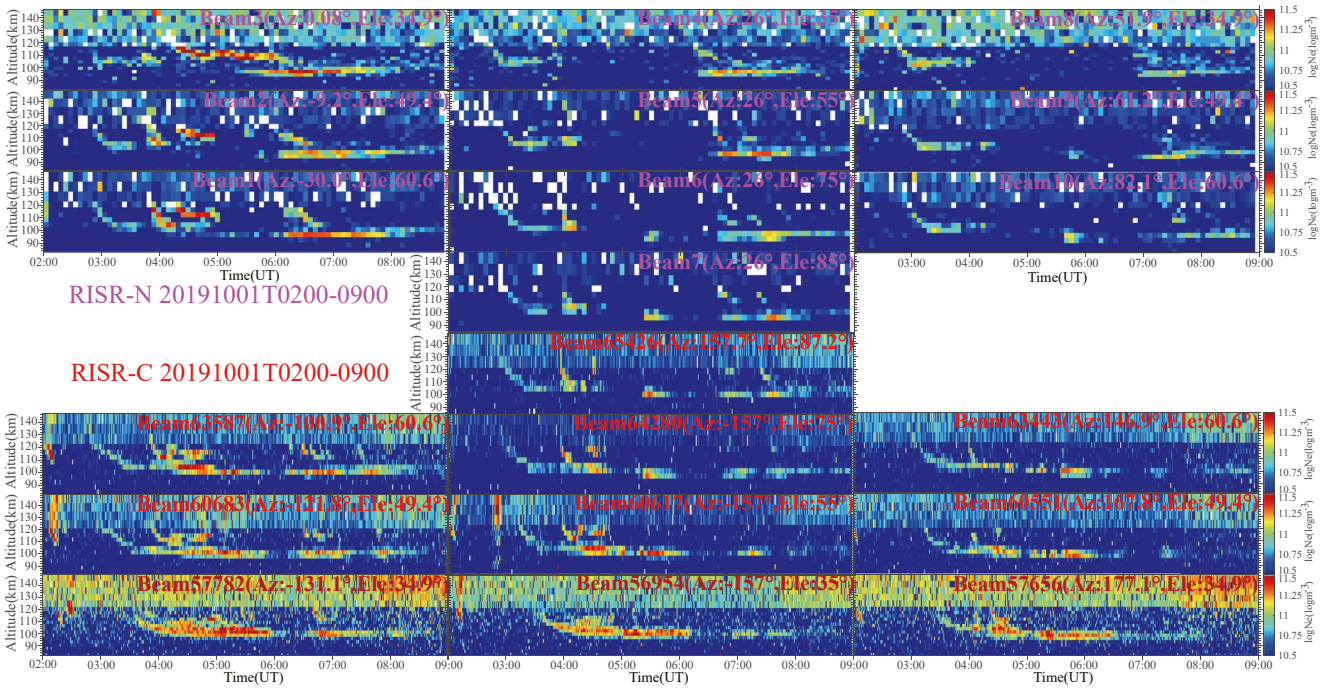

Figure 4. Examples of electron density profiles from the twin incoherent scatter radars of northward-looking face of Resolute Incoherent-Scatter Radar (RISR-N) (top panels) and Resolute Incoherent-Scatter Radar-Canada (RISR-C) (bottom panels) in an altitude of 80–150 km during the conducted period of 02:00–09:00 UT on 1 October 2019 at Resolute, Canada. All panels share one range as shown by the color-bar on the right-hand side. The beam number is labeled in the top-right corner of each panel, magenta for RISR-N, red for RISR-C, as well as their corresponding elevation and azimuth angles.

intersected points at an assumed altitude can be roughly estimated, which is simply considered as the horizontal scale of the polar cap Es layer. For the description of the adopted mathematic method in detail, please refer to Wang, Jayachandran, et al. (2021). Here, the assumed altitude is supposed to be 100 km at where the polar cap Es layer often occurs. Finally, the largest distance between these intersected points is ∼350 km, corresponding to between Beam 4 of RISR-N and Beam 56954 of RISR-C, as well as a similar value on the other direction. As a consequence, the horizontal scale of the polar cap Es layer is likely greater than 350 km, which is consistent with the reported scale of the Es layer at middle latitudes by Maeda and Heki (2015). Here, although we have extended the scale of the polar cap Es layer, we still request many dense observations (like from dense ground-based GPS receivers) in the future to accurately determine it over high latitudes.

Additionally, the signatures of the polar cap Es layer in detail will be continued. Close to the profile of Beam 65426 in Figure 4 (as an example), the initial sector of the polar cap Es layer is likely connecting to the lower F region above 150 km in altitude. In practice, there are many more examples as shown in Figure 4 to demonstrate the mentioned opinion, for example, the panels of Beam 60617 and 63443 and so on. It suggests that the concentration of metallic ions over high latitudes is probably related to the F region. Moreover, Figure 3 provides one more positive evidence to support it. At 02:40 UT (the beginning of polar cap Es layer), the virtual height of echoes reaches to >150 km, which is fundamentally consistent with the observations from Figure 4. After the formation of the polar cap Es layer, at around 04:00 UT there is a clear second generation of polar cap Es layer incompletely from the panels of Beams 1–3 of RISR-N and of Beams 63587 and 60683 and 57782 of RISR-C in Figure 4. After formed, the second polar cap Es layer is initially drifting to 110 km from 120 km in altitude and then is lasting stably from 04:00–07:00 UT, which is following the similar behavior of the first polar cap Es layer. It is interesting to point out that the appearance altitude of the second polar cap Es layer is approximately 10 km higher than the first one. Regarding the generation mechanism of the first and second polar cap Es layers and also the relations between these two different Es layers, more works should be carried out in near future. Referring to the issue at mid-latitudes, several enlightening mechanisms have been proposed to explain the formation of double Es layers, which are usually synthesized from a couple of possible forces, such as the neutral wind and the electric field and the gravity wave. During the SEEK-2 campaign (Sporadic-E Experiment over Kyushu 2), Wakabayashi and Ono (2005) examined the effects of wind shear and electric field on the generation of the multiple

Es layers, showing that the neutral wind shear is mainly responsible for the formation of the lower Es layer, meanwhile, the electric field provide a significant contribution to the generation of the upper layer. Moreover, Didebulidze et al. (2020) demonstrated that the atmospheric gravity waves under a specific condition can form multiple Es layers in theoretically and numerically. Therefore, these results may clue in interpreting the formation of double polar cap Es layers.

4. Discussion

This section is designed as two portions, briefly addressing the morphology of the polar cap Es layer at first, and then discussing the possible generation mechanism plainly.

4.1. The Morphology of Polar Cap Es Layer

As mentioned in the section of the Introduction, a large number of studies have focused on the characteristics of the Es layer at the middle latitude region. However, over the polar region, we still know little about it (even on the spatial characteristics), which is suffered from the scarce observation measurements, eagerly requesting further investigation.

In this paper, we are directly and comprehensively investigating the structures of the polar cap Es layer from a unique event observed by the twin incoherent scatter radars of RISR-N and RISR-C and CADI simultaneously. Making use of the vast view distance between 20 beams of the twin radars (Figure 4), the horizontal size of the polar cap Es layer is extended to greater than 350 km, which is first reported. Moreover, the multiple electron density profiles provide a large number of important information. Regarding the formation of the polar cap Es layer, the initial section of the polar cap Es layer is usually connecting to the lower F region (>150 km), presenting a piece of direct and firm evidence to prove the postulate of Chen et al. (2021). This peculiar manner instructively inspires the possible generation mechanism. After formed, the polar cap Es layer is staying a long time peacefully (>6 hr) until gradually vanished. The dynamics of the polar cap Es layer are also supported by the CADI observation (Figure 3). Note that the full appearance of the polar cap Es layer is recorded by CADI rather than the twin radars due to the lower density of polar cap Es layer during these gaps possibly attenuated by some functions. Furthermore, we also discover a new phenomenon of double Es layers at divided altitudes over the polar cap region, which has been reported at low latitude region from Digisonde and Very High Frequency radar (e.g., Xie et al., 2020 and references therein). However, it should be pointed out that the double Es layers have not been captured by the ionograms of Resolute CADI co-located with the twin ISR radars. The absence can be explained by two possible reasons. First, the altitude difference between the double Es layers is around 10 km from ISR radars, which is almost reaching the height resolution of CADI. Secondly, it is also likely that, even if the double layers are overhead at the CADI location, the upper layer would be blanketed by the layer below and we may thereby not see the upper layer at all.

4.2. A Newly Proposed Generation Process

In literature, several models have been proposed to explain the Es layer at high latitudes (e.g., Bristow & Watkins, 1991; Kirkwood & Collis, 1989; MacDougall & Jayachandran, 2005; MacDougall et al., 2000b; Nygrén et al., 2006), here some of which will be discussed in detail. First, the high-frequency appearance of the Es layer over a "cusp latitude" station is reasonably explained by the two-step mechanisms, including the horizontal convergence of ionization by the electric field of convection reversal at first, and then vertical convergence of these ionizations by the electric field in the polar cap (e.g., Chen et al., 2021; MacDougall & Jayachandran, 2005). However, as pointed out by the authors, it can only be suitable to a very narrow strip at high latitudes due to the strictly required terms of the electric field. As mentioned, the Resolute station is at the central polar cap, which is far away from the "cusp" region. In our case, during the period to organize polar cap Es layer (at ∼03:00 UT), the IMF Bz/By components are always negative/positive, respectively, probably inducing stable anti-sunward convection over the polar cap. We have checked the convection pattern derived from SuperDARN observations (not shown here), not finding supportive convection reversals around Resolute.

Secondly, at high latitudes, the view that gravity waves modulate the ionization then to make the Es layer is popular, which has been proposed and verified (e.g., Kirkwood & Collis, 1989; MacDougall et al., 2000a). MacDougall

et al. (2000b) proposed a gravity wave model that initially transports ionization out of the lower F region into the *E* region and then converges them by vertical wave motion, which was concluded from the drifting measurements of CADI and also simulations. Compared with our observations from the twin radars in Figure 4, the ionization of initial polar cap Es layer is drifting from the lower F region into the *E* region, which is strongly supported by CADI of Figure 3. On the other hand, during the period that the polar cap Es layer occurred, the parameters of positive IMF By component and also the UT hour range (03–09 UT) are overall following the statistical results from MacDougall et al. (2000a). Furthermore, in these papers, they concluded that the appearance of the polar cap Es layer is always related to the weak convection velocity, which is restricted by the properties of gravity waves. In our experiment, the convection velocity across Resolute is ∼250 m/s, which is estimated from the SuperDARN convection map, basically satisfying this condition. As a consequence, the gravity wave is suggested to be a candidate driver to form the polar cap Es layer despite lacking direct evidence. Unfortunately, CADI did not record the drift measurement due to a faulty antenna.

Moreover, the vertical motion of the polar cap Es layer had been speculated as combined effects from the electric field and neutral wind (e.g., Bristow & Watkins, 1991; Nygrén et al., 1984). Here only the potential driver of the electric field is discussed due to the observation limitation. The electric field mechanism has been heavily studied through the use of theoretical models (e.g., Bedey & Watkins, 1997, 1998; Kirkwood & von Zhan, 1991; Machuga & Mathews, 2001; Nygrén et al., 2006). Meanwhile, its effective directions have been studied in detail, possibly preferring to be directed in the N-W quadrant (e.g., Abdu et al., 2014; Bristow & Watkins, 1993, 1994; Parkinson et al., 1998; Voiculescu et al., 2006; Wan et al., 1999). However, the vertical transportation due to the electric field is proportional to the cos(*I*). In the central polar cap, the magnetic dip (*I*) approaches 90° (e.g., 88.8° of Resolute station), likely producing relatively weak vertical convergence under a common condition with weak horizontal velocity (e.g., Kirkwood & Collis, 1989; MacDougall et al., 2000a). Expectedly, this small vertical component is not strong enough to efficiently concentrate the polar cap Es layer. Nevertheless, Figure 2e provides evidence to suggest the presence of strong electric fields. The E component of the local magnetic field (black line in Figure 2e) rapidly decreases, strongly suggesting the current induced by the electric field, which coincides with the primary initial formation of the polar cap Es layer exactly. After that, the E component gradually returns to quiet conditions (around 0 nT at 08:00 UT). However, in Figure 4 (e.g., Beam 63587/60683/57782), the polar cap Es layers are initiated four separate times, such as at ∼03:00 UT, ∼04:00, ∼07:00, and ∼08:00 UT. Without the activity of the electric field, one must explain the other three initiation processes.

As a result, a new process, not a new mechanism, is tentatively proposed to explain the sophisticated issue of how to form the polar cap Es layer. It is widely accepted that gravity waves can be easily generated by the Joule heating associated with the auroral particle precipitation (caused by an electric field) (e.g., Bristow et al., 1994; Kirkwood & Collis, 1989). In practice, in the central polar cap (e.g., at Resolute station), particle precipitation is also possibly occurring, which is usually linked to the vertical electric field. Similarly, the gravity wave can be produced as well. Admittedly, the gravity wave would like to originate from the auroral oval, requiring further determination in the future. From the combined effects of electric field and gravity wave, the polar cap Es layer can be created if the metallic ions are abundant. This developed process can explain the repeatedly occurred formation of the polar cap Es layer from the effects of continued gravity waves.

5. Conclusions

In this paper, an interesting polar cap Es layer event is presented by using the comprehensive observations at Resolute Bay station, including the twin incoherent scatter radars of RISR-N and RISR-C, for the first time. CADI and magnetometer data are further used to support the observations from the dual ISRs. During this experiment, a case of polar cap Es layer that was observed on both incoherent scatter radars at the same time is presented. From the joint measurements, the morphological characteristics of the polar cap Es layer are developed in-depth. The horizontal scale of the polar cap Es layer is greater than 350 km, according to the multiple beams of the twin incoherent scatter radars. From the observed electron density profiles, the initial portion of the polar cap Es layer is found to likely be drifting from the lower F region (>150 km in altitude). Moreover, a unique phenomenon of double polar cap Es layer is presented from a couple of beams of the twin radars. As far as the authors are aware, it is the first time to demonstrate the peculiar activities of the polar cap Es layer. To explain the distinct phenomena, the appropriate mechanisms or processes are addressed in detail. After that, a simple process of the localized electric field and gravity wave is proposed. However, it needs further substantiation using more examples in the

future. As a consequence, much work should be conducted to expand the understanding of the polar cap Es layer that often occurs at high latitudes, which is potentially harmful to navigations and communications (e.g., Wang, Jayachandran, et al., 2021).

Data Availability Statement

The data of northward-looking face of Resolute Incoherent-Scatter Rada and Resolute Incoherent-Scatter Radar-Canada is collected from the madrigal database (http://cedar.openmadrigal.org/). The data of Canadian Advanced Digital Ionosonde is provided by the Canadian High Arctic Ionospheric Network from the database (http://chain.physics.unb.ca/chain/). The solar wind and Interplanetary Magnetic Field data are obtained from the OmniWeb (http://omniweb.gsfc.nasa.gov/html/sc_merge_data1.html). The SYM-H index is acquired from the World Data Center for Geomagnetism, Kyoto (http://wdc.kugi.kyoto-u.ac.jp/). The auroral electrojet indices of SME/SMU/SML and the perturbations of the magnetic field are collected from SuperMAG (https://supermag.jhuapl.edu/).

Acknowledgments
This work is supported by the National Natural Science Foundation of China (grants No. 42120104003, 41874170, and 41831072), China Postdoctoral Science Foundation funded project (2020M682163), Stable-Support Scientific Project of China Research Institute of Radiowave Propagation (A132101W02) and the Independent Research of China Aerospace Science and Technology Corporation (Y-KC-JT-00-026). The authors acknowledge the use of northward-looking face of Resolute Incoherent-Scatter Radar (RISR-N) and Resolute Incoherent-Scatter Radar-Canada (RISR-C) data. The Resolute Bay Observatory is a US National Science Foundation (NSF) research station, operated by SRI International. The observatory is home to NSF's RISR-N, and the University of Calgary's RISR-C. We thank the Physics department of the University of New Brunswick for running Canadian High Arctic Ionospheric Network (CHAIN). Infrastructure funding for the CHAIN was provided by the Canadian Foundation for Innovation and the New Brunswick Innovation Foundation. Science funding is provided by the Natural Sciences and Engineering Research Council of Canada.

References

Abdu, M. A., de Souza, J., Batista, I., Santos, A., Sobral, J., Rastogi, R., & Chandra, H. (2014). The role of electric fields in sporadic E layer formation over low latitudes under quiet and magnetic storm conditions. *Journal of Atmospheric and Terrestrial Physics*, *115–116*, 95–105. https://doi.org/10.1016/j.jastp.2013.12.003

Bedey, D. F., & Watkins, B. J. (1996). Seasonal occurrence of thin metallic ion layers at high latitudes. *Geophysical Research Letters*, *23*(20), 2789–2792. https://doi.org/10.1029/96GL02569

Bedey, D. F., & Watkins, B. J. (1997). Large-scale transport of metallic ions and the occurrence of thin ion layers in the polar ionosphere. *Journal of Geophysical Research*, *102*(A5), 9675–9681. https://doi.org/10.1029/96JA03825

Bedey, D. F., & Watkins, B. J. (1998). Diurnal occurrence of thin metallic ion layers in the high-latitude ionosphere. *Geophysical Research Letters*, *25*(20), 3767–3770. https://doi.org/10.1029/1998GL900035

Behnke, R. A., & Vickery, J. F. (1975). Radar evidence for Fe^+ in a sporadic-E layer. *Radio Science*, *10*(3), 325–327. https://doi.org/10.1029/RS010i003p00325

Bristow, W. A., Greenwald, R. A., & Samson, J. C. (1994). Identification of high-latitude acoustic gravity wave sources using the Goose Bay HF radar. *Journal of Geophysical Research*, *99*(A1), 319–331. https://doi.org/10.1029/93JA01470

Bristow, W. A., & Watkins, B. J. (1991). Numerical simulation of the formation of thin ionization layers at high latitudes. *Geophysical Research Letters*, *18*(3), 404–407. https://doi.org/10.1029/90GL02588

Bristow, W. A., & Watkins, B. J. (1993). Incoherent scatter observations of thin ionization layers at Sondrestrom. *Journal of Atmospheric and Terrestrial Physics*, *55*(6), 873–894. https://doi.org/10.1016/0021-9169(93)90028-W

Bristow, W. A., & Watkins, B. J. (1994). Effect of the large-scale convection electric field structure on the formation of thin ionization layers at high latitudes. *Journal of Atmospheric and Terrestrial Physics*, *56*(3), 401–415. https://doi.org/10.1016/0021-9169(94)90221-6

Chen, X., Huang, W., Ban, C., Kosch, M. J., Murphy, D. J., Hu, Z., et al. (2021). Dynamic properties of a sporadic sodium layer revealed by observations over Zhongshan, Antarctica: A case study. *Journal of Geophysical Research*, *126*(11), e2021JA029787. https://doi.org/10.1029/2021JA029787

Didebulidze, G. G., Dalakishvili, G., & Todua, M. (2020). Formation of multilayered sporadic E under an influence of atmospheric gravity waves (AGWs). *Atmosphere*, *11*(6), 653. https://doi.org/10.3390/atmos11060653

Fukao, S., Yamamoto, M., Tsunoda, R. T., Hayakawa, H., & Mukai, T. (1998). The SEEK (Sporadic-E experiment over Kyushu) campaign. *Geophysical Research Letters*, *25*(11), 1761–1764. https://doi.org/10.1029/98GL00932

Hysell, D. L., Munk, J., & McCarrick, M. (2014). Sporadic E ionization layers observed with radar imaging and ionospheric modification. *Geophysical Research Letters*, *41*(20), 6987–6993. https://doi.org/10.1002/2014GL061691

Jayachandran, P. T., Hamza, A., Hosokawa, K., Mezaoui, H., & Shiokawa, K. (2017). GPS amplitude and phase scintillation associated with polar cap auroral forms. *Journal of Atmospheric and Terrestrial Physics*, *164*, 185–191. https://doi.org/10.1016/j.jastp.2017.08.030

Jayachandran, P. T., Hosokawa, K., MacDougall, J. W., Mushini, S., Langley, R. B., & Shiokawa, K. (2009). GPS total electron content variations associated with a polar cap arc. *Journal of Geophysical Research*, *114*(A12), A12304. https://doi.org/10.1029/2009JA014916

Jayachandran, P. T., Langley, R. B., MacDougall, J. W., Mushini, S. C., Pokhotelov, D., Hamza, A. M., et al. (2009). Canadian high Arctic ionospheric Network (CHAIN). *Radio Science*, *44*(1), RS0A03. https://doi.org/10.1029/2008RS0040046

Kirkwood, S., & Collis, P. (1989). Gravity wave generation of simultaneous auroral sporadic-E layers and sudden neutral sodium layers. *Journal of Atmospheric and Terrestrial Physics*, *51*(4), 259–269. https://doi.org/10.1016/0021-9169(89)90077-9

Kirkwood, S., & von Zhan, U. (1991). On the role of auroral electric fields in the formation of low altitude Sporadic-E and sudden sodium layers. *Journal of Atmospheric and Terrestrial Physics*, *53*(5), 389–407. https://doi.org/10.1016/0021-9169(91)90034-5

Kumar, S., & Hanson, W. B. (1980). The morphology of metallic ions in the upper atmosphere. *Journal of Geophysical Research*, *85*(A12), 6783–6801. https://doi.org/10.1029/JA085iA12p06783

Larsen, M. F., Hysell, D. L., Zhou, Q. H., Smith, S. M., Friedman, J., & Bishop, R. L. (2007). Imaging coherent scatter radar, incoherent scatter radar, and optical observations of quasiperiodic structures associated with Sporadic E layers. *Journal of Geophysical Research*, *112*(A6), A06321. https://doi.org/10.1029/2006JA012051

Liou, K., Newell, P. T., Meng, C. I., Brittnacher, M., & Parks, G. (1998). Characteristics of the solar wind controlled auroral emissions. *Journal of Geophysical Research*, *103*(A8), 17543–17558. https://doi.org/10.1029/98JA01388

MacDougall, J. W., & Jayachandran, P. T. (2005). Sporadic E at cusp latitudes. *Journal of Atmospheric and Terrestrial Physics*, *67*(15), 1419–1426. https://doi.org/10.1016/j.jastp.2005.07.011

MacDougall, J. W., Jayachandran, P. T., & Plane, J. M. C. (2000a). Polar cap sporadic-E: Part1, observation. *Journal of Atmospheric and Terrestrial Physics*, *62*(13), 1155–1167. https://doi.org/10.1016/S1364-6826(00)00093-6

MacDougall, J. W., Jayachandran, P. T., & Plane, J. M. C. (2000b). Polar cap sporadic-E: Part2, modelling. *Journal of Atmospheric and Terrestrial Physics*, *62*(13), 1169–1176. https://doi.org/10.1016/S1364-6826(00)00092-4

Machuga, D. W., & Mathews, J. D. (2001). Numerical simulations of three-dimensional E-region ion trajectories in realistic tidal wind and E-field structures: Layer formation and transport. *Journal of Atmospheric and Terrestrial Physics*, *63*(14), 1519–1528. https://doi.org/10.1016/S1364-6826(01)00033-5

Maeda, J., & Heki, K. (2014). Two-dimensional observations of midlatitude Sporadic E irregularities with a dense GPS array in Japan. *Radio Science*, *49*(1), 28–35. https://doi.org/10.1002/2013RS005295

Maeda, J., & Heki, K. (2015). Morphology and dynamics of daytime mid-latitude sporadic-E patches revealed by GPS total electron content observations in Japan. *Earth Planets and Space*, *67*(1), 89. https://doi.org/10.1186/s40623-015-0257-4

Maeda, J., Suzuki, T., Furuya, M., & Heki, K. (2016). Imaging the midlatitude sporadic E plasma patches with a coordinated observation of spaceborne InSAR and GPS total electron content. *Geophysical Research Letters*, *43*(4), 1419–1425. https://doi.org/10.1002/2015GL067585

Narcisi, R. S. (1971). Composition studies of the lower thermosphere. In F. Veriani (Ed.), *Physics of upper atmosphere* (pp. 12–59). Editrice Compositori Publisher.

Newell, P. T., & Gjerloev, J. W. (2011a). Evaluation of SuperMAG auroral electrojet indices as indicators of substorms and auroral power. *Journal of Geophysical Research*, *116*(A12), A12211. https://doi.org/10.1029/2011JA016779

Newell, P. T., & Gjerloev, J. W. (2011b). Substorm and magnetosphere characteristic scales inferred from the SuperMAG auroral electrojet indices. *Journal of Geophysical Research*, *116*(A12), A12232. https://doi.org/10.1029/2011JA016936

Nygrén, T., Aikio, A. T., Voiculescu, M., & Ruohoniemi, J. M. (2006). IMF effect on sporadic-E layers at two northern polar cap sites: Part II–Electric field. *Annales Geophysicae*, *24*(3), 901–913. https://doi.org/10.5194/angeo-24-901-2006

Nygrén, T., Jalonen, L., Oksman, J., & Turunen, T. (1984). The role of electric field and neutral wind direction in the formation of sporadic E-layers. *Journal of Atmospheric and Terrestrial Physics*, *46*(4), 373–381. https://doi.org/10.1016/0021-9169(84)90122-3

Parkinson, M. L., Dyson, P., Monselesan, D., & Morris, R. (1998). On the role of electric field direction in the formation of sporadic E-layers in the southern polar cap ionosphere. *Journal of Atmospheric and Terrestrial Physics*, *60*(4), 471–491. https://doi.org/10.1016/S0273-1177(01)00037-0

Shinagawa, H., Miyoshi, Y., Jin, H., & Fujiwara, H. (2017). Global distribution of neutral wind shear associated with sporadic E layers derived from GAIA. *Journal of Geophysical Research: Space Physics*, *122*(4), 4450–4465. https://doi.org/10.1002/2016JA023778

Sun, W., Ning, B., Hu, L., Yue, X., Zhao, X., Lan, J., et al. (2020). The evolution of complex Es observed by multi instruments over low-latitude China. *Journal of Geophysical Research: Space Physics*, *125*(8), e2019JA027656. https://doi.org/10.1029/2019JA027656

Sun, W., Ning, B., Yue, X., Li, G., Hu, L., Chang, S., et al. (2018). Strong Sporadic E occurrence detected by ground-based GNSS. *Journal of Geophysical Research: Space Physics*, *123*(4), 3050–3062. https://doi.org/10.1002/2017JA025133

Sun, W., Zhao, X., Hu, L., Yang, S., Xie, H., Chang, S., et al. (2021). Morphological characteristics of thousand-kilometer-scale Es structures over China. *Journal of Geophysical Research: Space Physics*, *126*(2), e2020JA028712. https://doi.org/10.1029/2020JA028712

Turunen, T., Nygren, T., Huuskonen, A., & Jalonen, L. (1988). Incoherent scatter studies of Sporadic-E using 300 m resolution. *Journal of Atmospheric and Terrestrial Physics*, *50*(4–5), 277–287. https://doi.org/10.1016/0021-9169(88)90014-1

Voiculescu, M., Aikio, A. T., Nygrén, T., & Ruohoniemi, J. M. (2006). IMF effect on Sporadic-E layers at two northern polar cap sites: Part I–Statistical study. *Annales Geophysicae*, *24*(3), 887–900. https://doi.org/10.5194/angeo-24-887-2006

Wakabayashi, M., & Ono, T. (2005). Multi-layer structure of mid-latitude Sporadic-E observed during the SEEK-2 campaign. *Annales Geophysicae*, *23*, 2347–2355. SRef-ID: 1432-0576/ag/2005-23/2347. https://doi.org/10.5194/angeo-23-2347-2005

Wan, W. X., Parkinson, M., Dyson, P., Breed, A., & Morris, R. (1999). A statistical study of the interplanetary magnetic field control of Sporadic E-layer occurrence in the southern polar cap ionosphere. *Journal of Atmospheric and Terrestrial Physics*, *61*(18), 1357–1366. https://doi.org/10.1016/S1364-6826(99)00092-9

Wang, Y., Cao, Z., Xing, Z.-Y., Zhang, Q.-H., Jayachandran, P. T., Oksavik, K., et al. (2021). GPS scintillations and TEC variations in association with a polar cap arc. *Journal of Geophysical Research: Space Physics*, *126*(3), e2020JA028968. https://doi.org/10.1029/2020JA028968

Wang, Y., Hong, M. H., Chen, G. X., Xu, W., Du, A., Zhao, X., et al. (2010). Nightside field-aligned current during the April 6, 2000 superstorm. *Chinese Science Bulletin*, *55*(20), 2175–2181. https://doi.org/10.1007/s11434-010-3260-y

Wang, Y., Jayachandran, P. T., Themens, D. R., McCaffrey, A. M., Zhang, Q.-H., David, S., & Chadwick, R. (2021). A case study of polar cap sporadic-E layer associated with TEC variations. *Remote Sensing*, *13*(7), 1324. https://doi.org/10.3390/rs13071324

Wu, D. L., Ao, C. O., Hajj, G. A., de la Torre Juarez, M., & Mannucci, A. J. (2005). Sporadic E morphology from GPS CHAMP radio occultation. *Journal of Geophysical Research*, *110*(A1), A01306. https://doi.org/10.1029/2004JA010701

Xie, H., Li, G., Zhao, X., Ding, F., Yan, C., Yang, G., & Ning, B. (2020). Coupling between E region quasi-periodic echoes and F region medium-scale traveling ionospheric disturbances at low latitudes. *Journal of Geophysical Research*, *123*(5), e2019JA027720. https://doi.org/10.1029/2019JA027720

Yeh, W.-H., Liu, J.-Y., Huang, C.-Y., & Chen, S.-P. (2014). Explanation of the Sporadic-E layer formation by comparing FORMOSAT-3/COSMIC data with meteor and wind shear information. *Journal of Geophysical Research: Atmospheres*, *119*(8), 4568–4579. https://doi.org/10.1002/2013JD020798